Title page:

Exosomes exploit the virus entry machinery and pathway to transmit IFN-α-induced antiviral activity.

Zhenlan Yao[a], Xiaofang Li[a], Jieliang Chen[a], Yunsheng Qiao[a], Fang Shen[a], Bisheng Shi[b], Jia Liu[a], Jiahui Ding[a], Lu Peng[a], Jianhua Li[a]#, Zhenghong Yuan[a]#

[a] Key Laboratory of Medical Molecular Virology, School of Basic Medical Sciences, Shanghai Medical College of Fudan University, Shanghai, China

[b] Shanghai Public Health Clinical Center, Shanghai Medical College of Fudan University, China

Running Title: Exosome entry machinery and pathway into hepatocyte.

Address correspondence to Jianhua Li and Zhenghong Yuan, zhyuan@shmu.edu.cn.

Zhenlan Yao and Xiaofang Li contributed equally to this work.

Abstract

Interferon-α (IFN-α) induces the transfer of resistance to hepatitis B virus (HBV) from liver nonparenchymal cells (LNPCs) to hepatocytes via exosomes. However, little is known about the entry machinery and pathway involved in the transmission of IFN-α-induced antiviral activity. Here, we found that macrophage exosomes depend on T cell immunoglobulin and mucin receptor 1 (TIM-1), a hepatitis A virus (HAV) receptor, to enter hepatocytes for delivering IFN-α-induced anti-HBV activity. Moreover, two primary endocytic routes for virus infection, clathrin-mediated endocytosis (CME) and macropinocytosis, collaborate to permit exosome entry and anti-HBV activity transfer. Subsequently, lysobisphosphatidic acid (LBPA), an anionic lipid closely related to endosome penetration of virus, facilitates membrane fusion of exosomes in late endosomes/ multivesicular bodies (LEs/MVBs) and the accompanying exosomal cargo uncoating. Together, this study provides comprehensive insights into the transmission route of macrophage exosomes to efficiently deliver IFN-α-induced anti-HBV activity and highlights the similarities between the entry mechanisms of exosomes and virus.

Importance

Our previous study showed that LNPC-derived exosomes could transmit IFN-α-induced antiviral activity to HBV replicating hepatocytes, but the concrete transmission mechanisms which include exosome entry and exosomal cargo release remain unclear. In this study, we found that virus entry machinery and pathway were also applied to

exosome-mediated cell-to-cell antiviral activity transfer. Macrophage-derived exosomes exploit hepatitis A virus receptor for access to hepatocytes. Later, CME and macropinocytosis are utilized by exosomes which is followed by exosome-endosome fusion for efficient transfer of IFN-α-induced anti-HBV activity. Dissecting the similarities between exosome and virus entry will be beneficial to designing exosomes as efficient vehicles for antiviral therapy.

Introduction

Hepatitis B virus (HBV) is a small, enveloped DNA virus that replicates via an RNA intermediate and belongs to the Hepadnaviridae family(1). Approximately 400 million people are chronically infected with HBV worldwide(2). Chronic HBV infection is a major risk factor for the development of liver cirrhosis and hepatocellular carcinoma(3). Interferon (IFN)-α is licensed for the treatment of HBV chronic infection, with a response rate of 30-40% and a clinical cure rate of approximately 10%(4), but its efficacy is limited in hepatocytes (5, 6). We and others previously reported that IFN-α induced the transfer of resistance to hepatitis viruses from nonpermissive liver nonparenchymal cells (LNPCs), including liver resident macrophages, to permissive hepatocytes via exosomes, but the underlying mechanism remains largely unclear(7-11).

Exosomes are 40–100 nm membrane vesicles derived from the intraluminal vesicles (ILVs) of multivesicular bodies (MVBs) that are secreted into the extracellular milieu through the fusion of MVBs with the plasma membrane(12, 13). These vesicles can serve as mediators of intercellular communication to exchange functional proteins, lipids, mRNAs and microRNAs (miRNAs) among cells(14-16). Given the emerging roles of exosomes from IFN-α-induced LNPCs in the antiviral innate response and their therapeutic potential(7, 8, 17, 18), it is important to understand the molecular mechanisms by which nonparenchymal cell-derived exosomes are taken up into hepatocytes and release their cargo to inhibit HBV replication.

The entry strategy used by a given exosome may depend on the proteins and lipids on the surfaces of both exosomes and recipient cells(19-21). The routes and fates of

exosome internalization may partially overlap with those of the virus(9, 22, 23). Here, we found that the hepatitis A virus receptor, TIM-1, mediated the internalization of macrophage-derived exosomes into hepatocytes; we showed that the rapid clathrin-dependent pathway in concert with sustained macropinocytosis, two primary pathways for virus invasion, were also used as the major endocytic routes for exosome entry and the transmission of IFN-α-induced HBV resistance. After internalization, membrane fusion of exosomes and accompanying exosomal cargo uncoating took place in LEs/MVBs, relying on the LE-specific anionic lipid lysobisphosphatidic acid (LBPA). Collectively, our findings demonstrate that macrophage exosomes require virus entry machinery and pathway for transmission of IFN-α-induced antiviral activity to combat HBV in hepatocytes.

Materials and methods

Antibodies, reagents and Chemical Inhibitors

Antibodies for LAMP-2 (sc-18822), EEA1 (sc-33585) and normal mouse IgG (sc-2025) were purchased from Santa Cruz Biotechnology. Antibodies for Alix (12422-1-AP), TSG101 (14497-1-AP), CD63 (25682-1-AP), RAB5 (11947-1-AP) and RAB7 (55469-1-AP) were purchased from Proteintech Group (Rosemont, USA). Antibody for clathrin heavy chain (ab21679) was from Abcam (Cambridge, USA). Antibodies for β-actin (A2228) and GFP (G6539) were from Sigma-Aldrich. Antibody for LBPA (MABT837) was from EMD Millipore (Billerica, USA). Fluorescent secondary antibodies (A11001, A10523) were purchased from Invitrogen. Annexin V -FITC

(640905) was purchased from Biolegend (San Diego, USA). Phalloidin-iFluor 488 (23115) was from AAT Bioquest (Sunnyvale, USA). Fc-TIM-1-His, a protein of TIM-1 extracellular domain (AAC39862.1) (Ser 21-Gly 290) which is fused with a polyhistidine tag at the C-terminus and the Fc region of human IgG1 at the N-terminus was from Sino Biological (Beijing, China). Aldehyde/Sulfate Latex Beads(4% w/v, 4 μm) was from Invitrogen (Carlsbad, USA).

Chemical inhibitors including dynasore (D7693), MβCD (C4555), EIPA (A3085), IPA-3 (I2285) and rottlerin (R5648) were from Sigma-Aldrich. Filipin III (70440) was purchased from Cayman chemical (Ann Arbor, USA). Chlorpromazine (S2456) and nystatin (S1934) were purchased from Selleck Chemicals (Houston, USA).

Cells, plasmids, siRNAs and transfection

The HepG2.2.15, HepG2 and THP-1 cells used in this study have been described previously(7, 24). HepG2.2.15 and HepG2 cells were cultured in DMEM with 10% fetal bovine serum (FBS) (Biologic Industries, Beit Haemek, Israel) and Penicillin-Streptomycin (Invitrogen, Carlsbad, USA), while THP-1 cells were maintained in RPMI-1640 with 10% FBS and antibiotics. To obtain macrophage-like cells that closely resembled human monocyte-derived macrophages, THP-1 cells were differentiated via PMA stimulation (phorbol 12-myristate 13-acetate; Sigma-Aldrich, Taufkirchen, Germany), as described previously(7, 25).

Markers of endosomal compartments fused with cyan fluorescent protein (CFP), including CFP-RAB5, CFP-RAB7 and CFP-CD63, were kindly provided by Walther Mothes from Yale University in New Haven, CT, USA(26). K44A dynamin-2 pEGFP was

a gift from Sandra Schmid (Addgene plasmid # 34687). pcDNA3-EGFP-Cdc42-T17N (Addgene plasmid # 12976) and pcDNA3-EGFP-Rac1-T17N (Addgene plasmid # 12982) were gifts from Gary Bokoch. Caveolin-1 labeled with C-terminal tag of enhanced green fluorescent protein (EGFP) was constructed by insertion of the claveolin-1 cDNA fragment into a pEGFP-N1 expression vector (Clontech, Palo Alto, USA). To produce GFP-carrying exosomes, a THP-1 cell line stably expressing GFP was established via lentivirus transduction. The lentiviral vector PLJM1-GFP (Addgene) was used to generate lentivirus for the transduction, according to the manufacturer's instructions (Addgene). Stable GFP-expressing THP-1 cells were selected by flow cytometric sorting (BD FACSAria II; BD Biosciences, San Jose, USA). siRNAs for clathrin heavy chain, caveolin-1 and negative control were purchased from Santa Cruz Biotechnology. siRNA for TIM-1 was purchased from Ruibo.

DNA plasmid transfection into HepG2 cells was performed using Lipofectamine 2000 (Invitrogen). For RNA-mediated interference, HepG2 cells at 30 to 40% confluence were transfected with 50 nM small interfering RNA (siRNA) duplexes designed and purchased from Santa Cruz (Dallas, USA) or Ruibo (Guangzhou, China) using RNAiMAX (Invitrogen) according to the manufacturer's instructions. At 24 h post-transfection, the cells were transfected again with 50 nM of the same siRNA duplexes. The following treatment was performed 72 h after the first siRNA transfection.

Exosome purification, characterization and labeling

Macrophages derived from THP-1 or GFP-expressing THP-1 cells were grown in culture medium supplemented with 10% FBS (which was depleted of endogenous

138 exosomes by overnight centrifugation at 100,000 g). Exosomes from the culture
139 supernatants were isolated by differential centrifugation, as described previously(7). To
140 obtain exosomes from IFN-α-treated macrophages, the macrophages were treated for
141 48 h with 1,000 U/ml of IFN-α (PBL Assay Science, New Brunswick, USA) before
142 isolation. The purified exosomes were characterized via electron microscopy and
143 immunoblot analysis, as described previously(7). Protein amounts of exosomes were
144 quantified using a BCA protein assay kit (Pierce, Rockford, USA).

145 The isolated exosomes were labeled with PKH67 or PKH26 according to the
146 manufacturer's protocol (Sigma-Aldrich) for use in endocytosis assays. For the
147 fluorescence self-quenching assay for membrane fusion, R18 (Octadecyl Rhodamine B
148 Chloride, Invitrogen) was inserted into the viral membranes at a self-quenching surface
149 density(27, 28).

150 **Endocytosis assays of exosomes**

151 To assay exosome internalization, 10-20 μg/ml of labeled exosomes were added to
152 HepG2 cells cultured with serum-free medium and incubated at 37℃. HepG2 cells were
153 untreated or pretreated with the indicated amounts of inhibitors for 30 min before
154 incubation with exosomes or endocytic markers. Except cholesterol inhibitors (MβCD,
155 nystatin, and filipin III), inhibitory compounds were present continuously during
156 subsequent endocytosis assays. Despite moderate cytotoxicity of MβCD-treated cells,
157 no significant toxicity was observed for the other inhibitors (data not shown), which
158 indicated that inhibition of exosome internalization was not caused by cytotoxicity. As
159 controls, HepG2 cells were incubated with 2 μg/ml of Alexa568-transferrin (Invitrogen) or

160 0.2 mg/ml of dextran labeled with Rhodamine B isothiocyanate (RhoB-dextran,
161 Sigma-Aldrich) for 30 min or 1 h at 37℃. For competitive inhibition of TIM-1-mediated
162 exosome entry by Fc-TIM-1-His, HepG2 cells were incubated with labeled exosomes in
163 presence of 1 μg/ml Fc-TIM-1-His at 37℃ for 2 h. Endocytosis was stopped, and
164 surface-bound exosomes or markers were removed by washing with ice-cold PBS.

165 **Confocal laser-scanning and time-lapse microscopy**

166 Confocal images were captured using a Leica TCS SP8 confocal microscope (Leica
167 Microsystems, Buffalo Grove, USA) with a 400X or 630X oil objective (pinhole set at 1
168 Airy unit) and processed using LAS X (Leica). For time-lapse microscopy analysis,
169 HepG2 cells were grown in 35-mm glass bottom culture dishes with four chambers
170 (Cellvis, Mountain View, USA) overnight. Before microscopic examination, the medium
171 was changed to serum-free DMEM, and fluorescence-labeled exosomes were added
172 and kept in the medium during image collection. Time-lapse images were captured every
173 10 min for 6-μm slices using a DeltaVision Elite high-resolution microscope (Applied
174 Precision, Issaquah, USA) connected to a 37°C incubator and buffered with 5% CO_2.
175 The images were further processed with softWoRx Explorer (Applied Precision,
176 Issaquah, USA) and analyzed with ImageJ (NIH, USA). For colocalization studies, the
177 distribution patterns of the fluorescent signals were analyzed using the Plot Profile
178 analysis tool of ImageJ, and Pearson's correlation coefficients (Rr) were obtained by
179 using the Colocalization finder plugin of ImageJ. For the Pearson's correlation
180 coefficients (Rr), the values ranged from 1 (a perfect positive correlation) to −1 (a perfect
181 negative correlation), with 0 representing a random distribution(29). Time-related

fluorescence intensities of the R18 dequenching signals were assessed using the Time Series Analyzer V3 plugin of ImageJ.

Flow cytometry analysis

For endocytosis assay, cells were washed three times with ice-cold PBS, detached using trypsin, and subsequently resuspended in PBS with 1% FBS. Flow cytometry analysis was performed on an LSR Fortessa instrument integrated with the FACSDiva software (BD Biosciences). A minimum of 10,000 events within the gated live cells were collected and analyzed per sample using FlowJo (Tree Star, Ashland, USA).

For PtdSer detection, 4 μm latex beads were coated with exosomes through 2-hour incubation at room temperature. The exosome-bead complexes were then blocked with 200 mM glycine and normal IgG and washed with 1% FBS which was followed by annexin V-FITC labeling for 40 min at 4℃. The exosome-bead complexes were subsequently washed and suspended with 1% FBS for flow cytometry analysis. A minimum of 50,000 events within the gated exosome-bead complexes were collected and analyzed per sample via FlowJo.

HBV DNA quantitation and antigen measurement

HepG2.2.15 cells pre-transfected with siRNAs or pretreated with chemical inhibitors were incubated with exosomes isolated from macrophages with or without IFN-α treatment at a concentration of 10 μg/ml for 48 h. The supernatant of the HepG2.2.15 culture was collected and transferred for viral antigen measurement using the enzyme-linked immunosorbent assay (Kehua ELISA kit; Kehua, Shanghai, China). HBV DNA levels in the culture medium were extracted using a MagNA Pure 96 system (Roche,

204 Shanghai, China) and quantified using real-time PCR.

205 **Statistics**

206 All data are presented as the mean of duplicates ± S.D. Statistical comparisons

207 were made using a two-tailed Student's t-test; *P* values of 0.05 or less were considered

208 to be statistically significant.

209

Results

PtdSer receptor TIM-1 is necessary for exosome entry and the transfer of IFN-α-induced anti-HBV activity

Exosomes were isolated from the culture of THP-1-derived macrophages by differential centrifugation, as described previously(7). Membrane vesicles approximately 100 nm in diameter with a cup-shaped structure typical of exosomes were identified by electron microscopy (Fig. 1A). Further characterization by immunoblotting indicated the presence of exosomal markers (CD63, TSG101, and Alix), conserved exosomal proteins (LAMP-2, β-actin) and the absence of the endosomal marker EEA1 (Fig. 1B). Isolated exosomes were labeled with the fluorescent lipid dye PKH26 or PKH67. We observed the internalization of PKH26-labeled exosomes by hepatocyte-derived HepG2 cells, which were stained for cytoskeletal F-actin with Phalloidin-iFluor 488 (Fig. 1C) at 37°C, and found that the uptake kinetics were time- and concentration-dependent (Fig. 1D).

PtdSer — an apoptosis marker typically located on the inner leaflet of the plasma membrane — is found on the outer membrane of exosomes from bone marrow derived dendritic cells (BMDCs) and oligodendrocytes(20, 30). Previous experimental evidence indicates that some viruses may exploit PtdSer as apoptotic disguise and enter target cells through PtdSer receptor-mediated internalization(31). To determine whether and which PtdSer receptors play a role in the entry of macrophage-derived exosomes into hepatocytes, we first confirmed PtdSer expression on the outer membrane of

231 macrophage-derived exosomes through annexin-V labeling of exosomes isolated from
232 macrophages (Fig. 1 E).
233 We then inhibited the expression of two hepatic PtdSer receptors involved in virus
234 entry(31), T cell immunoglobulin and mucin receptor 1 (TIM-1) (Fig. 1F) and Growth
235 Arrest Specific 6 (GAS6) (data not shown), in HepG2 cells with specific siRNAs. The
236 uptake of PKH26-labeled exosomes was significantly reduced in HepG2 cells after TIM-1
237 knockdown (Fig. 1G and H), but interference via GAS6 expression had no effect on
238 exosome uptake (data not shown). It is notable that the IgV in ectodomains of TIM
239 proteins bind PtdSer on viral envelope and enhance virus entry(32). Exogenous
240 Fc-TIM-1-His, TIM-1 extracellular domain fused with His tag and Fc region of human
241 IgG1, competitively inhibited exosome internalization by HepG2 cells (Figure 1I), which
242 suggested that the ectodomain of TIM-1 also play a functional role in exosome entry.
243 Corresponding to previous results reflecting the engagement of TIM-1 in exosome
244 uptake, IFN-α-induced anti-HBV activity mediated by exosomes from IFN-α-stimulated
245 macrophages (IFN-EXO) was diminished in TIM-1-knockdown HepG2.215 cells in
246 comparison to that in cells transfected with control (ctrl) siRNA, as indicated by HBsAg
247 expression (Fig. 1J). In addition, IFN-α-induced exosome-mediated antiviral activity only
248 slightly suppressed HBV DNA production in the supernatant of TIM-1-knockdown cells,
249 in contrast to cells transfected with ctrl siRNA (Fig. 1K). It was unexpected that the
250 knockdown of TIM-1 caused a decrease in HBV DNA in the supernatant, which suggests
251 that TIM-1 is a positive factor for HBV replication (Fig. 1K). Collectively, these findings
252 demonstrated that PtdSer and its receptor TIM-1 act as portals for exosomal

253 internalization and the transfer of IFN-α-induced antiviral activity against HBV.

254

255 **Dynamin-2 and cholesterol are required for exosome entry into hepatocytes**

256 The interaction of exosomes with receptors on donor cells can induce the cellular
257 response of internalization through endocytic pathways(33). Endocytosis occurs via
258 several pinocytic mechanisms that include the clathrin-mediated mechanism,
259 macropinocytosis, the caveolae-mediated mechanism and other less well-defined
260 mechanisms(34, 35). The large GTPase dynamin-2 functions at the heart of endocytic
261 vesicle fission in clathrin-mediated endocytosis (CME) and caveolae-mediated
262 endocytosis (Fig. 2A)(36). Recent studies showed that dynamin is also responsible for
263 the closure of circular ruffles in macropinocytosis (Fig. 2A)(37). Cholesterol plays
264 essential roles in the formation of caveolae, clathrin-coated pit budding and membrane
265 ruffling in macropinocytosis (Fig. 2A)(38-40).

266 To investigate the role of dynamin-2 in exosome entry, we suppressed the function
267 of dynamin-2 in HepG2 cells with the specific inhibitor dynasore. The efficacy of
268 dynasore was confirmed using Alexa568-labeled transferrin (Alexa568-TFN), which is
269 the best-characterized cargo protein of CME (Fig. 2B and C). The uptake of
270 PKH26-labeled exosomes was reduced by approximately 60% following dynasore
271 treatment (Fig. 2C). In addition, the expression of the dominant-negative mutant of
272 dynamin-2, Dyn2K44A, also significantly blocked exosome entry (Fig. 2D). We next
273 sought to determine whether cholesterol is necessary for exosome entry into
274 hepatocytes. Using Methyl-β-cyclodextran (MβCD) to extract cholesterol from the

plasma membrane of HepG2 cells significantly inhibited PKH26-labeled exosome entry (Fig. 2E and F). The reduction was up to 86% when treating HepG2 cells with 10 mM MβCD (Fig. 2 F). Masking cholesterol with binding compounds (nystatin and filipin) resulted in milder but still apparent inhibition of exosome uptake by HepG2 cells (Fig. 2E, G and H). These results indicated that the dynamin-2- and cholesterol-dependent endocytic pathways are required for the entry of exosomes into hepatocytes.

Clathrin- but not caveolae-mediated endocytosis is important for exosome uptake and the transmission of IFN-α-induced anti-HBV activity

CME, which is the uptake of material into cells from the surface using clathrin-coated vesicles, is the preferred route by which some PtdSer-exposing viruses enter target cells(31). To investigate the dependence of exosome entry on CME, hepatocytes were treated with chlorpromazine (CPZ), an inhibitor of clathrin-coated pit assembly. PKH26-labeled exosome uptake decreased by 34%, and as a positive control, transferrin uptake was inhibited under the same conditions (Fig. 3A and B). Moreover, knockdown of the clathrin heavy chain (CHC) also reduced exosome entry into hepatocytes by 34% (Fig. 3C and D). To further investigate the endocytic pattern engaged in exosome entry, exosomes were stained with PKH67 and administered to HepG2 cells in the presence of Alexa568-TFN. Partial colocalization of exosomes and transferrin was observed 30 min post-internalization, while little colocalization was captured 1 h after internalization, indicating rapid clathrin-dependent endocytosis during the early stage of exosome internalization (Fig. 3E and F). Scatterplots, Pearson's

297 correlation coefficient (Rr) and an intensity profile were used to quantify the degree of
298 colocalization between PKH67-labeled exosomes and Alexa568-TFN. Partial
299 colocalization between exosomes and transferrin was evidenced by scatterplots, a
300 fraction of which were close to diagonal, and the corresponding Rr was 0.1292 (see
301 Materials and Methods) (Fig. 3E). There were several peak superpositions in the
302 intensity profile (Fig. 3E). Correspondingly, the downregulation of CHC expression in
303 HBV-replicating hepatocytes weakened the IFN-α-induced anti-HBV activity transmitted
304 by exosomes in HepG2.2.15 cells, as indicated by viral antigen expression and DNA
305 quantification (Fig. 3G and H). In addition, caveolae-mediated endocytosis did not
306 appear to be required for exosome internalization by hepatocytes, as indicated by the
307 inhibition of caveolin-1 (CAV1) expression (Fig. 3I and J). Together, these data showed
308 that clathrin- but not caveolae-mediated endocytosis contributed to exosome uptake and
309 the transfer of IFN-α-induced HBV resistance.
310
311 **Macropinocytosis plays an alternative role in exosome uptake and the transfer of**
312 **IFN-α-induced anti-HBV activity**
313 More than one endocytic route was reported to be used in virus or exosome
314 entry(33, 41). Given the incomplete inhibition of exosome entry by blockade of CME and
315 the sustained increase of internalized exosomes for hours (Fig. 1D and 3B, D), there
316 might be alternative pathways to support exosome entry into hepatocytes.
317 Macropinocytosis is a fluid-phase type of endocytosis that is accompanied by membrane
318 ruffles regulated by actin rearrangement(37). This process is engaged in apoptotic cell

319 removal and is favored by some viruses that use apoptotic mimicry to enter target
320 cells(31).

321 The induction of a robust increase in fluid-phase uptake is a hallmark of
322 macropinocytosis(39). The results showed that the uptake of 70-kDa dextran labeled
323 with Rhodamine B isothiocyanate (RhoB-dextran), which is a fluid-phase marker specific
324 for macropinocytosis, was enhanced by incubation with macrophage-derived exosomes
325 in HepG2 cells (Fig. 4A). A Na+/H+ exchanger (NHE) is needed for macropinosome
326 formation via the modulation of Rho GTPases at the plasma membrane, and NHE
327 inhibition by 5-(N-Ethyl-N-isopropyl) amiloride (EIPA) has been widely used as a
328 diagnostic criterion for macropinocytosis(42). The entry of both exosomes and dextran
329 into HepG2 cells was apparently inhibited by EIPA, and a remarkable decrease (80%) in
330 exosome uptake was achieved in the presence of 80 nM EIPA (Fig. 4B and C). PAK1 and
331 PKC are two serine/threonine kinases that are required for macropinocytosis(39). We
332 found that exosome entry was markedly blocked by the PAK1 inhibitor IPA-3 and the
333 PKC inhibitor rottlerin (Fig. 4D-F). PKC inhibition resulted in a more significant reduction
334 in exosome internalization by up to 66% in hepatocytes (Fig. 4F). As a positive control,
335 dextran internalization was greatly inhibited by the two kinase inhibitors (Fig. 4 D-F).
336 However, the expression of a dominant-negative mutant of Rac1 or Cdc42, two common
337 GTPases that modulate membrane ruffles, had no effect on exosome internalization (Fig.
338 4G and H), which suggested that macrophage exosomes might enter hepatocytes via a
339 Rac1- or Cdc42-independent route. Next, we reinvestigated the role of macropinocytosis
340 in exosome entry by comparing the distribution patterns of dextran and exosomes after

341 internalization. In contrast to that seen for rapid CME-dependent exosome uptake,
342 confocal images showed consistent colocalization of PKH67-labeled exosomes with
343 RhoB-dextran-filled intracellular vacuoles (Fig. 4I and J). A highly overlapped distribution
344 was observed 1 h post-exosome internalization and was confirmed by the corresponding
345 scatterplots, colocalization coefficient and intensity profile (Fig. 4J). Furthermore, the
346 inhibition of macropinocytosis in HepG2.2.15 cells by EIPA partially blocked the
347 IFN-α-induced anti-HBV activity mediated by exosomes derived from IFN-treated
348 macrophages, as indicated by viral DNA quantification (Fig. 4K). Thus, we concluded
349 that macropinocytosis served as a sustained alternative route that was active from the
350 early stage of exosome internalization and cooperated with CME to ensure hepatocytes
351 the access to exosome-mediated HBV resistance.
352
353 **Exosomes expose cargo through membrane fusion in late endosomes/**
354 **multivesuclar bodies**
355 Once internalized within primary endocytic vesicles, the incoming substances
356 traffic into the endosomal system(41). The endocytosed substances are routed from
357 early endosomes (EEs) to late endosomes (LEs, often taking the form of MVBs) and
358 lysosomes for degradation(41). Membrane fusion-induced endosome penetration is
359 commonly manipulated by viruses or delivery vectors to send viral genomes or biologics
360 to the cytosol before lysosomal degradation(27, 43-45). It remains unknown whether a
361 similar membrane fusion strategy is adopted for exosomal cargo release in endosomes
362 after internalization (Fig. 5A).

We first used time-lapse microscopy to track membrane fusion events in live hepatocytes incubated with macrophage-derived exosomes prelabeled with self-quenching amounts of the hydrophobic dye rhodamine C18 (R18). R18 is commonly used as a fluorescent probe to detect virus-induced membrane fusion. The probe is incorporated into membranes at high concentrations to cause self-quenching, and dequenching of the probe occurs when membrane fusion decreases in density(27, 28). The dequenching signal of membrane fusion was first captured approximately 45 minutes after treating HepG2 cells with R18-labeled exosomes, and fusion events followed within 1 hour (Fig. 5B). The fluorescence intensity profile showed persistent enhanced R18 fluorescence for the fusion spots (Fig. 5C).

EEs and LEs/MVBs are major fusion sites for some viruses to deliver nucleocapsids and release nucleocapsids to the cytosol(46). To locate the exact site at which membrane fusion occurred after exosome internalization, we performed colocalization experiments using a variety of endosomal markers. Endosomal compartments in HepG2 cells were labeled via transient transfection of plasmids encoding CFP-fused markers for EEs (RAB5), LEs/MVBs (RAB7) and intraluminal vesicles (ILVs) in MVBs (CD63). The dequenching signal of membrane fusion was colocalized with the LE marker CFP-RAB7 and the ILV marker CFP-CD63 in live HepG2 cells after treatment with R18-labeled exosomes, while no colocalization was observed with markers for EEs (CFP-RAB5) (Fig. 5D). Hence, LEs/MVBs might be the proper site for the membrane fusion of macrophage-derived exosomes after exosome internalization.

385 To track exosomal cargo after membrane fusion, the live dynamics of exosomal
386 cargo in hepatocytes were tested by monitoring the membrane fusion events of
387 R18-labeled GFP-carrying exosomes using time-lapse microscopy, with exosomes
388 isolated from GFP-expressing macrophages. At the beginning of the experiment, orange
389 fluorescence was observed at the fusion site due to the combined fluorescence emitted
390 by dequenching R18 inserted into exosome membranes and GFP encapsulated in
391 exosomes. As fusion proceeded, the extreme dilution of the R18-labeled membrane
392 components increased the fluorescence of the gradually exposed GFP. A complete color
393 switch was accomplished when the exosomal cargo GFP was totally uncoated and
394 “released” (Fig. 5E). In addition, confocal images proved again that LEs were the site of
395 membrane fusion for GFP-carrying exosomes (Fig. 5F). The colocalization coefficient of
396 R18 and GFP was approximately 0.9 in HepG2 cells, indicating a high frequency of
397 fusion events among internalized exosomes. Together, these data indicated that
398 LEs/MVBs provided the proper conditions for exosome fusion and cargo uncoating,
399 which might promote exosomal cargo release based on endosome penetration.
400
401 **Lysobisphosphatidic acid (LBPA) contributes to exosome fusion and the**
402 **uncoating of exosomal cargo**
403 Anionic lipids are beneficial for endosome penetration(46). A high concentration of
404 anionic lipids makes LEs a suitable location for endosome leakage via membrane fusion.
405 Notably, the LE-specific anionic lipid LBPA assists as both viruses and delivery vectors to
406 achieve efficient cytosolic access via membrane fusion-induced endosome

penetration(43-48).

The accumulation of PKH26-labeled exosomes in the LBPA-rich structure suggested a potential interaction between the two components (Fig. 6A). Partial colocalization between the dequenching R18 of exosomes and LBPA signals indicated the participation of LBPA in the membrane fusion of exosomes in LEs/MVBs (Fig. 6B). To verify the dependence of exosome fusion on LBPA, HepG2 cells were pre-incubated with an anti-LBPA blocking antibody(27, 43), and the dequenching signals of R18-labeled exosomes were tracked via time-lapse microscopy. Pretreatment with an anti-LBPA blocking antibody produced significant inhibition of membrane fusion, as suggested by the decayed R18 dequenching of exosomes (Fig. 6C). The fluorescent intensity profile of tracked fluorescent puncta further manifested the dependence of exosome fusion on LBPA (Fig. 6D). To inquire into the contribution of LBPA to the potential intracellular release of exosomal cargo before lysosomal degradation, we incubated LBPA-blocked HepG2 cells with GFP-carrying exosomes and judged the delivery efficiency of exosomal cargo to lysosomes based on the colocalization efficiency between GFP and lysosomes. The incidence of colocalization increased significantly in cells pretreated with the anti-LBPA blocking antibody, as indicated by the 2-fold increase in the colocalization coefficient (0.5487) in comparison to control cells (Fig. 6E). This finding suggested that some exosomal cargo might escape from endosomes to avoid lysosomal degradation via LBPA-dependent membrane fusion in LEs/MVBs. Unfortunately, the blocking of LBPA in HepG2.2.15 cells led to a four-fold increase in HBV DNA in the supernatant, suggesting that LBPA is closely related to HBV replication (Fig. 6F). This outcome

429 impeded further investigations of LBPA in exosome-mediated antiviral activity
430 transmission. Taken together, LBPA is very important for exosome fusion and the
431 uncoating of exosomal cargo.
432

433 Discussion

434 In this report, we demonstrate that macrophage-derived exosomes utilize virus entry
435 machinery and pathway to proffer IFN-α-induced HBV resistance to hepatocytes. We
436 have presented evidence that macrophage exosomes engage TIM-1, a PtdSer receptor,
437 to enter hepatocytes and undergo rapid CME or sustained macropinocytosis. Our data
438 also suggest that LEs/MVBs are the primary location for LBPA-mediated exosome fusion
439 and accompanying exosomal cargo uncoating for potential intracellular release. The
440 endocytic pathway and membrane fusion in endosomes provide an ideal strategy for
441 exosomes from IFN-α-induced macrophages to deliver antiviral activity and control HBV
442 replication in hepatocytes (Fig. 7).

443 Exosomes have been shown to interact with membrane receptors on target cells to
444 facilitate subsequent endocytosis(33). Recently, a virus endocytic model ─ apoptotic
445 mimicry ─ was suggested to play a role in exosome entry(9, 31). As former ILVs form by
446 inward budding of the LE/MVB-limiting membrane, exosomes are thought to expose
447 PtdSer, an apoptotic marker, on the external leaflet of the membrane and initiate PtdSer
448 receptor-engaged uptake(49). Apoptotic mimicry has been used by hepatotropic
449 hepatitis A virus (HAV) for infection, in which the virus is cloaked in a PtdSer-containing

envelope by hijacking the exosome secretion pathway and entering target cells via TIM-1-mediated internalization(31, 50, 51). In this study, we verified PtdSer expression on the external membrane of macrophage exosomes and found that the knockdown of TIM-1 significantly blocked exosome entry and the transfer of IFN-α-induced HBV resistance into hepatocytes. These results indicate that macrophage exosomes may exploit an endocytic strategy similar to apoptotic mimicry as HAV uses to enter cells via TIM-1-mediated internalization. However, the possibility is not excluded that additional receptors may act as co-factors to enhance the attachment of exosomes onto hepatocytes for subsequent entry. Several adhesion molecules enriched on exosome surface, including integrins, immunoglobulins and proteoglycans, are reported to be involved in exosome attachment to cells(9, 21, 33), which implies the necessity of further study on co-receptors.

Adhesion to receptors commonly results in a cellular response of internalization through endocytic pathways(41). Experimental evidence implies important roles for various endocytic pathways in exosome entry, including CME, caveolae-mediated endocytosis, macropinocytosis and phagocytosis(22, 23, 30, 33). It is believed that various combinations of endocytic mechanisms are responsible for exosome entry in different cell types(33). PtdSer exposure is exploited by some viruses as apoptotic disguise which triggers subsequent CME or macropinocytosis for virus entry(31).

According to the results, macrophage exosome entry is sensitive to dynamin and cholesterol inhibitors. Dynamin mediates the fission of endocytic vesicles from the plasma membrane in several endocytic mechanisms, such as CME and

caveolae-mediated endocytosis(36). Recent research indicates that dynamin also regulates the closure of circular ruffles during macropinocytosis(37). Cholesterol is an essential constituent of functional domains on the membrane, including lipid rafts and caveolae(40, 41). Cholesterol is required for the formation of endocytic vesicle budding and membrane ruffling(38, 39).

Exosome entry was inhibited by CPZ or CHC knockdown. The rapid accumulation of exosomes and transferrin in the same transport intermediates affirmed that CME plays a role in early exosome uptake by hepatocytes. However, CAV1 knockdown had no effect on exosome internalization. Considering the low expression of CAV1 in HepG2 cells and primary hepatocytes(52), caveolae-mediated endocytosis may contribute little to exosome uptake by hepatocytes.

Furthermore, we found that EIPA, the hallmark inhibitor of macropinocytosis, blocked macrophage exosome entry into hepatocytes. The dependence of exosome entry on PAK1 and PKC was also validated based on the decreased internalization caused by the corresponding kinase inhibitors. In addition, the increasing colocalization of exosomes with dextran during exosome uptake implied that macropinocytosis serves as an efficient alternative route for sustained exosome entry. However, Rac1 and Cdc42, two Rho GTPases that are usually engaged in macropinocytosis, do not appear to be involved in macrophage exosome uptake by hepatocytes. This finding is inconsistent with the interference of exosome entry by EIPA, which inhibits the activation of Rac1 and Cdc42 by altering the sub-membranous pH(42). Therefore, exosome entry into hepatocytes may rely on undefined EIPA-sensitive Rho GTPases. Moreover, Rac1- and

494 Cdc42-independent macropinocytosis is reportedly invoked during influenza A virus (IAV)
495 entry(53). Related studies also showed that circular ruffling and macropinocytosis
496 independent of Rac1 or Cdc42 could be triggered by the non-receptor tyrosine kinase
497 c-src(54). The inhibition of CME or macropinocytosis attenuated exosome-mediated
498 IFN-α-induced anti-HBV transmission, which indicates that exosomes derived from
499 IFN-α-stimulated macrophages utilize both endocytic mechanisms to deliver HBV
500 resistance to HBV-replicating hepatocytes.

501 Little research to date has focused on the fates of exosomes and exosomal cargo
502 after internalization(9). Endocytosed substances are usually directed to the endosomal
503 system, where they are sorted, processed, recycled, stored and degraded(41). The
504 endosome system is primarily composed of EEs, recycling endosomes (REs), LEs and
505 lysosomes(41). LEs often take the form of MVBs. Invagination and inward budding of the
506 limiting membrane of LEs form ILVs (exosomes) within MVBs(55). Viruses and delivery
507 vectors exploit endosomes for penetration into the cytosol through membrane fusion to
508 deliver viral genomes or biologics(44-46).

509 Using a live cell imaging system and a fusion probe (R18), we found that LEs/MVBs
510 were also the potential site of exosome fusion initiation, followed by cargo uncoating.
511 Notably, the persistence of R18 dequenching signals for several minutes indicated that
512 exosome fusion was trapped in an endosomal sub-compartment, identical to the
513 colocalization of fusion signals with an ILV marker (CD63) (Fig. 5C and D)(27).

514 Previous studies have shown that a high concentration of anionic lipids in LEs
515 provides an appropriate environment for endosome penetration(46, 56). It was reported

516 that the presence of anionic lipids in the target membrane promoted membrane fusion
517 efficiency for some enveloped viruses(43, 47, 57). LBPA is a specific anionic lipid in LEs
518 and is thought to promote ILV budding and back-fusion(55, 58) during MVB biogenesis.
519 Research has suggested that the vesicular stomatitis virus (VSV) loads nucleocapsids
520 into ILVs through membrane fusion and penetrates LEs/MVBs through LBPA-dependent
521 back-fusion between the ILV membrane and the endosome-limiting membrane(43). In
522 addition, LBPA is also required for efficient cytosolic access of delivery vectors, including
523 dfTAT and phosphorothioate-modified antisense oligonucleotides (PS-ASO)(44, 45).

524 Our results showed that the fusion sites of exosomes were colocalized with LBPA.
525 Moreover, LBPA antibodies inhibited the membrane fusion of endocytosed exosomes
526 and accelerated the transport of exosomal cargo to lysosomes. It is possible that some
527 exosomal cargo may avoid lysosomal degradation via LBPA-dependent membrane
528 fusion in LEs/MVBs. Given the above results, we hypothesize that LBPA facilitated the
529 fusion of exosomes from IFN-α-stimulated macrophages with ILVs in LEs/MVBs and that
530 exosomal antiviral cargo are then reloaded into fused ILVs and released after
531 back-fusion with the limiting membrane of LEs/MVBs. As former ILVs formed in
532 LEs/MVBs, endocytosed exosomes with ILV properties may also be qualified for direct
533 fusion with the limiting membrane of LEs/MVBs to release cargo.

534 Overall, our results illustrate how receptors, endocytic pathways and
535 LBPA-dependent membrane fusion are exploited by macrophage exosomes to deliver
536 IFN-α-induced anti-HBV activities to hepatocytes. This study also highlights the overlap
537 between viruses and exosomes by identifying that the infection strategies of viruses are

538 also applied for exosome entry and exosomal cargo delivery. Dissecting the complete
539 endocytic routes of exosomes may provide a fundamental basis for engineering
540 exosomes as therapeutic vehicles to deliver antiviral molecules with high efficiency.
541

542 # Acknowledgments

543 We thank Zhigang Yi, Xiaonan Zhang for valuable comments and suggestions, and Lu
544 Bai, Xiaoting Du, Yaming Li, Ke Qiao, Shuhui Sun for technical assistance.
545 This work was supported by research grants from the National Natural Science
546 Foundation of China (81471932), the National Natural Science Foundation (91542207),
547 the National Key Research and Development Program of China (2016YFC1200400) and
548 Shanghai Rising-Star Program (14QA1400700).
549 The authors declare no competing financial interests.
550

551 # References

552 1. **Block TM, Guo H, Guo J-T.** Molecular Virology of Hepatitis B Virus for Clinicians. Clinics in
553 Liver Disease **11:**685-706.
554 2. **Shepard CW, Simard Ep Fau - Finelli L, Finelli L Fau - Fiore AE, Fiore Ae Fau - Bell BP, Bell BP.**
555 Hepatitis B virus infection: epidemiology and vaccination.
556 3. **Levrero M, Zucman-Rossi J.** 2016. Mechanisms of HBV-induced hepatocellular carcinoma.
557 Journal of Hepatology **64:**S84-S101.
558 4. **Loggi E, Vitale G, Conti F, Bernardi M, Andreone P.** 2015. Chronic hepatitis B: Are we close
559 to a cure? Dig Liver Dis **47:**836-841.
560 5. **Mutz P, Metz P, Lempp FA, Bender S, Qu B, Schoneweis K, Seitz S, Tu T, Restuccia A,**
561 **Frankish J, Dachert C, Schusser B, Koschny R, Polychronidis G, Schemmer P, Hoffmann K,**
562 **Baumert TF, Binder M, Urban S, Bartenschlager R.** HBV Bypasses the Innate Immune
563 Response and Does not Protect HCV From Antiviral Activity of Interferon. LID -
564 S0016-5085(18)30112-4 [pii] LID - 10.1053/j.gastro.2018.01.044 [doi].

6. **Suslov A, Boldanova T, Wang X, Wieland S, Heim MH.** Hepatitis B Virus Does Not Interfere with Innate Immune Responses in the Human Liver. LID - S0016-5085(18)30078-7 [pii] LID - 10.1053/j.gastro.2018.01.034 [doi].
7. **Li J, Liu K, Liu Y, Xu Y, Zhang F, Yang H, Liu J, Pan T, Chen J, Wu M, Zhou X, Yuan Z.** 2013. Exosomes mediate the cell-to-cell transmission of IFN-alpha-induced antiviral activity. Nat Immunol **14:**793-803.
8. **Giugliano S, Kriss M, Golden-Mason L, Dobrinskikh E, Stone AEL, Soto-Gutierrez A, Mitchell A, Khetani SR, Yamane D, Stoddard M, Li H, Shaw GM, Edwards MG, Lemon SM, Gale M, Shah VH, Rosen HR.** 2015. HCV Infection Induces Autocrine Interferon Signaling by Human Liver Endothelial Cell and Release of Exosomes, Which Inhibits Viral Replication. Gastroenterology **148:**392-402.e313.
9. **van Dongen HM, Masoumi N, Witwer KW, Pegtel DM.** 2016. Extracellular Vesicles Exploit Viral Entry Routes for Cargo Delivery. Microbiol Mol Biol Rev **80:**369-386.
10. **Klenerman P, Ramamurthy N.** Liver sinusoidal endothelial cells: an antiviral "defendothelium".
11. **Bordon Y.** Viral immunity: arms convoy.
12. **Thery C, Ostrowski M, Segura E.** 2009. Membrane vesicles as conveyors of immune responses. Nat Rev Immunol **9:**581-593.
13. **Izquierdo-Useros N, Puertas MC, Borras FE, Blanco J, Martinez-Picado J.** 2011. Exosomes and retroviruses: the chicken or the egg? Cell Microbiol **13:**10-17.
14. **Pegtel DM, Cosmopoulos K, Thorley-Lawson DA, van Eijndhoven MA, Hopmans ES, Lindenberg JL, de Gruijl TD, Wurdinger T, Middeldorp JM.** 2010. Functional delivery of viral miRNAs via exosomes. Proc Natl Acad Sci U S A **107:**6328-6333.
15. **Schorey JS, Bhatnagar S.** 2008. Exosome function: from tumor immunology to pathogen biology. Traffic **9:**871-881.
16. **Robbins PD, Morelli AE.** 2014. Regulation of Immune Responses by Extracellular Vesicles. Nature reviews Immunology **14:**195-208.
17. **Lai RC, Yeo RW, Tan KH, Lim SK.** 2013. Exosomes for drug delivery - a novel application for the mesenchymal stem cell. Biotechnol Adv **31:**543-551.
18. **van den Boorn JG, Schlee M, Coch C, Hartmann G.** 2011. SiRNA delivery with exosome nanoparticles. Nature Biotechnology **29:**325.
19. **Wei X, Liu C, Wang H, Wang L, Xiao F, Guo Z, Zhang H.** 2016. Surface Phosphatidylserine Is Responsible for the Internalization on Microvesicles Derived from Hypoxia-Induced Human Bone Marrow Mesenchymal Stem Cells into Human Endothelial Cells. PLoS One **11:**e0147360.
20. **Morelli AE, Larregina AT, Shufesky WJ, Sullivan ML, Stolz DB, Papworth GD, Zahorchak AF, Logar AJ, Wang Z, Watkins SC, Falo LD, Jr., Thomson AW.** 2004. Endocytosis, intracellular sorting, and processing of exosomes by dendritic cells. Blood **104:**3257-3266.
21. **Christianson HC, Svensson Kj Fau - van Kuppevelt TH, van Kuppevelt Th Fau - Li J-P, Li Jp Fau - Belting M, Belting M.** Cancer cell exosomes depend on cell-surface heparan sulfate proteoglycans for their internalization and functional activity. doi:D - NLM: PMC3808637 OTO - NOTNLM.
22. **Tian T, Zhu YL, Zhou YY, Liang GF, Wang YY, Hu FH, Xiao ZD.** 2014. Exosome uptake through clathrin-mediated endocytosis and macropinocytosis and mediating miR-21 delivery. J Biol

Chem **289:**22258-22267.

23. **Nanbo A, Kawanishi E, Yoshida R, Yoshiyama H.** 2013. Exosomes derived from Epstein-Barr virus-infected cells are internalized via caveola-dependent endocytosis and promote phenotypic modulation in target cells. J Virol **87:**10334-10347.
24. **Li J, Lin S Fau - Chen Q, Chen Q Fau - Peng L, Peng L Fau - Zhai J, Zhai J Fau - Liu Y, Liu Y Fau - Yuan Z, Yuan Z.** Inhibition of hepatitis B virus replication by MyD88 involves accelerated degradation of pregenomic RNA and nuclear retention of pre-S/S RNAs. doi:D - NLM: PMC2903248 EDAT- 2010/04/23 06:00 MHDA- 2010/06/30 06:00 CRDT- 2010/04/23 06:00 PHST- 2010/04/23 06:00 [entrez] PHST- 2010/04/23 06:00 [pubmed] PHST- 2010/06/30 06:00 [medline] AID - JVI.00236-10 [pii] AID - 10.1128/JVI.00236-10 [doi] PST - ppublish.
25. **Auwerx J.** The human leukemia cell line, THP-1: a multifacetted model for the study of monocyte-macrophage differentiation.
26. **Sherer NM, Lehmann MJ, Jimenez-Soto LF, Ingmundson A, Horner SM, Cicchetti G, Allen PG, Pypaert M, Cunningham JM, Mothes W.** 2003. Visualization of retroviral replication in living cells reveals budding into multivesicular bodies. Traffic **4:**785-801.
27. **Nour AM, Li Y, Wolenski J, Modis Y.** 2013. Viral membrane fusion and nucleocapsid delivery into the cytoplasm are distinct events in some flaviviruses. PLoS Pathog **9:**e1003585.
28. **Citovsky V Fau - Blumenthal R, Blumenthal R Fau - Loyter A, Loyter A.** Fusion of Sendai virions with phosphatidylcholine-cholesterol liposomes reflects the viral activity required for fusion with biological membranes.
29. **L Barlow A, Macleod A, Noppen S, Sanderson J, J Guérin C.** 2010. Colocalization Analysis in Fluorescence Micrographs: Verification of a More Accurate Calculation of Pearson's Correlation Coefficient, vol 16.
30. **Fitzner D, Schnaars M, van Rossum D, Krishnamoorthy G, Dibaj P, Bakhti M, Regen T, Hanisch UK, Simons M.** 2011. Selective transfer of exosomes from oligodendrocytes to microglia by macropinocytosis. J Cell Sci **124:**447-458.
31. **Amara A, Mercer J.** 2015. Viral apoptotic mimicry. Nature Reviews Microbiology **13:**461-469.
32. **Moller-Tank S, Albritton LM, Rennert PD, Maury W.** Characterizing functional domains for TIM-mediated enveloped virus entry.
33. **Mulcahy LA, Pink RC, Carter DR.** 2014. Routes and mechanisms of extracellular vesicle uptake. J Extracell Vesicles **3**.
34. **Doherty GJ, McMahon HT.** 2009. Mechanisms of endocytosis. Annu Rev Biochem **78:**857-902.
35. **Nonnenmacher M, Weber T.** 2011. Adeno-associated virus 2 infection requires endocytosis through the CLIC/GEEC pathway. Cell Host Microbe **10:**563-576.
36. **Antonny B, Burd C, De Camilli P, Chen E, Daumke O, Faelber K, Ford M, Frolov VA, Frost A, Hinshaw JE, Kirchhausen T, Kozlov MM, Lenz M, Low HH, McMahon H, Merrifield C, Pollard TD, Robinson PJ, Roux A, Schmid S.** 2016. Membrane fission by dynamin: what we know and what we need to know. The EMBO Journal **35:**2270-2284.
37. **Mercer J, Helenius A.** 2012. Gulping rather than sipping: macropinocytosis as a way of virus entry. Curr Opin Microbiol **15:**490-499.
38. **Subtil A, Gaidarov I Fau - Kobylarz K, Kobylarz K Fau - Lampson MA, Lampson Ma Fau - Keen JH, Keen Jh Fau - McGraw TE, McGraw TE.** Acute cholesterol depletion inhibits

clathrin-coated pit budding. doi:D - NLM: PMC21991 EDAT- 1999/06/09 00:00 MHDA- 1999/06/09 00:01 CRDT- 1999/06/09 00:00 PHST- 1999/06/09 00:00 [pubmed] PHST- 1999/06/09 00:01 [medline] PHST- 1999/06/09 00:00 [entrez] PST - ppublish.

39. **Mercer J, Helenius A.** 2009. Virus entry by macropinocytosis. Nat Cell Biol **11:**510-520.

40. **Branza-Nichita N, Macovei A, Lazar C.** 2012. Caveolae-Dependent Endocytosis in Viral Infection. doi:10.5772/48538.

41. **Mercer J, Schelhaas M, Helenius A.** 2010. Virus entry by endocytosis. Annu Rev Biochem **79:**803-833.

42. **Koivusalo M, Welch C, Hayashi H, Scott CC, Kim M, Alexander T, Touret N, Hahn KM, Grinstein S.** 2010. Amiloride inhibits macropinocytosis by lowering submembranous pH and preventing Rac1 and Cdc42 signaling. The Journal of Cell Biology **188:**547-563.

43. **Le Blanc I, Luyet PP, Pons V, Ferguson C, Emans N, Petiot A, Mayran N, Demaurex N, Faure J, Sadoul R, Parton RG, Gruenberg J.** 2005. Endosome-to-cytosol transport of viral nucleocapsids. Nat Cell Biol **7:**653-664.

44. **Erazo-Oliveras A, Najjar K, Truong D, Wang TY, Brock DJ, Prater AR, Pellois JP.** 2016. The Late Endosome and Its Lipid BMP Act as Gateways for Efficient Cytosolic Access of the Delivery Agent dfTAT and Its Macromolecular Cargos. Cell Chem Biol **23:**598-607.

45. **Wang S, Sun H, Tanowitz M, Liang X-h, Crooke ST.** 2017. Intra-endosomal trafficking mediated by lysobisphosphatidic acid contributes to intracellular release of phosphorothioate-modified antisense oligonucleotides. Nucleic Acids Research **45:**5309-5322.

46. **White JM, Whittaker GR.** 2016. Fusion of Enveloped Viruses in Endosomes. Traffic **17:**593-614.

47. **Roth SL, Whittaker GR.** 2011. Promotion of vesicular stomatitis virus fusion by the endosome-specific phospholipid bis(monoacylglycero)phosphate (BMP). FEBS Letters **585:**865-869.

48. **Farzan M, Pasqual G, Rojek JM, Masin M, Chatton J-Y, Kunz S.** 2011. Old World Arenaviruses Enter the Host Cell via the Multivesicular Body and Depend on the Endosomal Sorting Complex Required for Transport. PLoS Pathogens **7:**e1002232.

49. **Thery C, Zitvogel L Fau - Amigorena S, Amigorena S.** Exosomes: composition, biogenesis and function.

50. **Kaplan G, Totsuka A, Thompson P, Akatsuka T, Moritsugu Y, Feinstone SM.** 1996. Identification of a surface glycoprotein on African green monkey kidney cells as a receptor for hepatitis A virus. Embo j **15:**4282-4296.

51. **Ramakrishnaiah V, van der Laan LJW.** 2014. Hepatitis virus hijacks shuttle: Exosome-like vesicles provide protection against neutralizing antibodies. Hepatology **59:**2416-2418.

52. **Cokakli M, Erdal E, Nart D, Yilmaz F, Sagol O, Kilic M, Karademir S, Atabey N.** 2009. Differential expression of Caveolin-1 in hepatocellular carcinoma: correlation with differentiation state, motility and invasion. BMC Cancer **9:**65.

53. **Pekosz A, de Vries E, Tscherne DM, Wienholts MJ, Cobos-Jiménez V, Scholte F, García-Sastre A, Rottier PJM, de Haan CAM.** 2011. Dissection of the Influenza A Virus Endocytic Routes Reveals Macropinocytosis as an Alternative Entry Pathway. PLoS Pathogens **7:**e1001329.

54. **Mettlen M, Platek A Fau - Van Der Smissen P, Van Der Smissen P Fau - Carpentier S,**

Carpentier S Fau - Amyere M, Amyere M Fau - Lanzetti L, Lanzetti L Fau - de Diesbach P, de Diesbach P Fau - Tyteca D, Tyteca D Fau - Courtoy PJ, Courtoy PJ. Src triggers circular ruffling and macropinocytosis at the apical surface of polarized MDCK cells.

55. **Piper RC, Katzmann DJ.** 2007. Biogenesis and function of multivesicular bodies. Annu Rev Cell Dev Biol **23:**519-547.

56. **Matos PM, Marin M, Ahn B, Lam W, Santos NC, Melikyan GB.** 2013. Anionic lipids are required for vesicular stomatitis virus G protein-mediated single particle fusion with supported lipid bilayers. J Biol Chem **288:**12416-12425.

57. **Zaitseva E, Yang ST, Melikov K, Pourmal S, Chernomordik LV.** 2010. Dengue virus ensures its fusion in late endosomes using compartment-specific lipids. PLoS Pathog **6:**e1001131.

58. **Matsuo H, Chevallier J Fau - Mayran N, Mayran N Fau - Le Blanc I, Le Blanc I Fau - Ferguson C, Ferguson C Fau - Faure J, Faure J Fau - Blanc NS, Blanc Ns Fau - Matile S, Matile S Fau - Dubochet J, Dubochet J Fau - Sadoul R, Sadoul R Fau - Parton RG, Parton Rg Fau - Vilbois F, Vilbois F Fau - Gruenberg J, Gruenberg J.** Role of LBPA and Alix in multivesicular liposome formation and endosome organization.

Figure legends

Figure 1. TIM-1 mediates exosome internalization and IFN-α-induced anti-HBV activity transmission.

(A) Electron microscopy of purified exosomes from macrophages. Scale bar: 100 nm.

(B) Immunoblot analysis of macrophage-derived exosomes (left) and corresponding cells (right) for exosomal and non exosomal markers.

(C) PKH26-labeled exosome internalization by HepG2 cells. Scale bar: 5 μm.

(D) Time- and concentration-dependent uptake of exosomes. HepG2 cells were incubated with PKH67-labeled exosomes (PKH67-EXO) at the indicated concentrations for up to 10 h (right). The fluorescence intensity distribution of cells incubated with PKH67-EXO for 3 h is also shown (left).

(E) PtdSer detection on the exosome surface. Exosomes coated onto 4 μM latex beads were either stained or not with Annexin V-FITC and analyzed by flow cytometry.

(F) Knockdown validation of TIM-1 by immunoblot.

(G, H) Confocal images (G) or flow cytometry analysis (H) of PKH26-labeled exosome internalization by HepG2 cells after TIM-1 knockdown. Scale bars: 10 μm. For flow cytometry analysis, both histogram graph (left) and mean fluorescence intensities (MFI) (right) which are normalized to siCTRL-transfected cells are presented.

(I) Flow cytometry analysis of PKH26-labeled exosome internalization by HepG2 cells in presence or absence (Ctrl) of Fc-TIM-1-His. MFI (right) are normalized to ctrl cells.

(J, K) Blockade of IFN-α-induced anti-HBV activity transmission by TIM-1 knockdown. HepG2.2.15 cells transfected with either siTIM-1 or siCTRL were treated with exosomes from IFN-α-stimulated macrophages (IFN-EXO) or unstimulated cells (Ctrl-EXO). HBsAg and HBV DNA levels in the medium were measured by ELISA (J) or quantified by qPCR (K).

The error bars indicate the SD. $*P < 0.05$, $**P < 0.01$, $***P < 0.001$, $****P < 0.0001$ (Student's t-test). The data are representative of three independent experiments.

Figure 2. Exosome internalization is dynamin- and cholesterol-dependent.

(A) Schematic representation of the roles of dynamin-2 and cholesterol in various endocytic pathways.

(B, C) Confocal images (B) or flow cytometry analysis (C) of exosome and transferrin internalization by HepG2 cells treated with dynasore. Scale bars: 10 μm. MFI (right) are normalized to DMSO-treated cells.

(D) Flow cytometry analysis of exosome internalization by HepG2 cells transfected with EGFP-Dyn2K44A mutant. HepG2 cells transfected with EGFP-tagged

748 dominant-negative dynK44A mutant were incubated with PKH26-labeled exosomes.
749 Transfected cells (EGFP+) are gated, and the uptake of exosomes among transfected
750 cells (EGFP+/PKH26+) is analyzed and presented by histogram graph (left) and MFI
751 (right). MFI are normalized to vector-transfected controls.

752 **(E-H)** Confocal images (E) or flow cytometry analysis (F-H) of exosome internalization
753 by HepG2 cells treated with cholesterol inhibitors (MβCD, Nystatin and Filipin). Scale
754 bars: 10 μm. For flow cytometry analysis, MFI (right) are normalized to DMSO-treated
755 cells.

756 The error bars indicate the SD. **P* < 0.05, ***P* < 0.01, ****P* < 0.001 (Student's t-test). The
757 data are representative of three independent experiments.

758 **Figure 3. Exosome internalization involves clathrin-mediated endocytosis (CME)**
759 **not caveolae-mediated endocytosis.**

760 **(A, B)** Confocal images (A) or flow cytometry analysis (B) of exosome and transferrin
761 internalization by HepG2 cells treated with 10 μg/ml CPZ. Scale bars: 10 μm. For flow
762 cytometry analysis, MFI (right) are normalized to DMSO-treated cells.

763 **(C)** Knockdown validation of clathrin heavy chain (CHC) by immunoblot.

764 **(D)** Flow cytometry analysis of exosome internalization by HepG2 cells after CHC
765 knockdown. MFI (right) are normalized to siCTRL-transfected cells.

766 **(E, F)** Internalized exosome colocalized with transferrin 30 (E) min or 1 h (F) after
767 internalization. The cells were fixed and analyzed by confocal microscopy. Scatterplots
768 and Pearson's correlation coefficients for the overlap of red (Alexa568-transferrins) and
769 green (PKH67-labeled exosomes) pixel intensities corresponding to the images are

770 presented. Intensity profiles are used to describe the distribution along the indicated
771 white arrow in the region of interest (ROI). Scale bars: 5 μm.

772 **(G, H)** Blockade of IFN-α-induced anti-HBV activity transmission by CHC knockdown.
773 HepG2.2.15 cells transfected with either siCHC or siCTRL were treated with IFN-EXO or
774 Ctrl-EXO. HBsAg and HBV DNA levels in the medium were measured by ELISA (G) or
775 quantified by qPCR (H).

776 **I** Knockdown validation of caveolin-1 (CAV1) by immunoblot. Endogenous amount of
777 caveolin-1 in HepG2 cells is low. To test the knock-down efficiency, siRNAs with a
778 plasmid encoding EGFP-CAV1 were cotransfected. Expression of EGFP-CAV1 was
779 assessed by immunoblot.

780 **J** Flow cytometry analysis of exosome internalization by HepG2 cells with CAV1
781 knocked down. MFI (right) are normalized to siCTRL-transfected cells.

782 The error bars indicate the SD. *P < 0.05, ****P < 0.0001 (Student's t-test). The data are
783 representative of three independent experiments.

784 **Figure 4. Exosome internalization involves macropinocytosis.**

785 **(A)** Preincubation with exosomes increased dextran uptake in HepG2 cells.
786 RhoB-dextran (RhoB-DEX) uptake by HepG2 cells pretreated with exosomes (EXO(+))
787 was analyzed by flow cytometry ,and the MFI is normalized to untreated cells (EXO(-)).

788 **(B, C)** Confocal images (B) or flow cytometry analysis (C) of exosome and dextran
789 internalization by HepG2 cells treated with EIPA. Scale bars: 10 μm. For flow cytometry
790 analysis, MFI (right) are normalized to DMSO-treated cells.

791 **(D-F)** Confocal images (D) or flow cytometry analysis (E, F) of exosome and dextran

792 internalization by HepG2 cells treated with IPA-3 or rottlerin. Scale bars: 10 μm. For flow
793 cytometry analysis, MFI (right) are normalized to DMSO-treated cells.
794 **(G, H)** Exosome uptake is independent of Rac1 or Cdc42. Flow cytometry analysis of
795 exosome internalization by HepG2 cells transfected with EGFP-Rac1 DN mutant (G) or
796 EGFP-Cdc42 DN mutant (H), followed by the incubation with PKH26-labeled exosomes.
797 Transfected cells (EGFP+) are gated, and the uptake of exosomes among transfected
798 cells (EGFP+/PKH26+) is analyzed as described above.
799 **(I, J)** Internalized exosome colocalized with dextran 30 min (I) or 1 h (J) after
800 internalization. The colocalization of Rho-dextran (red) with PKH67-labeled exosomes
801 (green) is analyzed as described above. Scale bars: 5 μm.
802 **(K)** Blockade of IFN-α-induced anti-HBV activity transmission by EIPA treatment.
803 HepG2.2.15 cells were pretreated with DMSO or EIPA which presented continuously
804 during following incubation with IFN-EXO or Ctrl-EXO. HBV DNA levels in the medium
805 were quantified by qPCR.
806 The error bars indicate the SD. *P < 0.05, **P < 0.01, ****P < 0.0001 (Student's t-test).
807 The data are representative of three independent experiments.
808 **Figure 5. Membrane fusion of GFP-carrying exosomes occurs in LEs/MVBs.**
809 **(A)** Hypothesized model of exosome fusion and cargo release in endosomes.
810 **(B)** Images of R18 dequenching triggered by exosome membrane fusion.
811 R18-dequenching fusion spots (red) were tracked and imaged at the indicated time
812 points via time-lapse microscopy. Scale bars: 5 μm.
813 **(C)** Time-intensity profiles of R18 fluorescence of two representative dequenching

814 spots in experiment (B).

815 **(D)** Membrane fusion signals of exosomes colocalized with the LE marker CFP-RAB7
816 and the ILV marker CFP-CD63. Dynamic colocalization events of dequenching signals
817 (red) with cellular markers (CFP pseudo-colored green) were tracked via time-lapse
818 microscopy. Scatterplots and Pearson's correlation coefficients for colocalization are
819 presented below the images. Scale bars: 5 μm.

820 **(E)** Color shift induced by ongoing fusion process of GFP-carrying exosomes
821 prelabeled with self-quenching concentrations of R18 was observed and imaged via
822 time-lapse microscopy. Scale bars: 5 μm.

823 **(F)** Membrane fusion signals of GFP-carrying exosomes colocalized with the LE
824 marker RAB7. Scatterplots and Pearson's correlation coefficient between the signals of
825 GFP and R18 or the signals of R18 and RAB7 are presented. Fluorescence intensity
826 profiles of GFP, RAB7 and R18 along the indicated white arrow in the ROI are also
827 presented. Scale bars: 10 μm.

828 **Figure 6. LBPA is required for exosome fusion and cargo uncoating.**

829 **(A)** Accumulation of PKH26-labeled exosomes in LBPA-rich vacuoles. Colocalization
830 of PKH26 (red) with LBPA (green) is analyzed as mentioned above. Scale bar: 10 μm.

831 **(B)** Membrane fusion signals of dequenching R18-exosomes colocalized with LBPA.
832 Colocalization of dequenching signals (red) with LBPA (green) is analyzed as described
833 above. Scale bars: 10 μm.

834 **(C)** Inhibition of exosome fusion by antibodies against LBPA. Fusion spots of
835 dequenching R18-exosomes in HepG2 cells pretreated with 50 μg/ml anti-LBPA or

836 anti-IgG overnight were tracked and photographed at the indicated time points. Scale
837 bars: 5 μm.

838 **(D)** Time-intensity profiles of R18 fluorescence of four representative dequenching
839 spots in experiment (C).

840 **(E)** Increase in colocalization of the exosomal cargo GFP with lysosomes after
841 exposure to antibodies against LBPA. HepG2 cells pretreated with anti-LBPA or anti-IgG
842 overnight were incubated with GFP-carrying exosomes in the presence of Lyso Tracker.
843 Colocalization of GFP (green) with lysosomes (red) is analyzed via scatterplots and
844 Pearson's correlation coefficients. Scale bars: 10 μm.

845 **Figure 7. Proposed model of exosome entry and delivery of IFN-α-induced HBV**
846 **resistance.**

847 After binding to TIM-1, exosomes from IFN-α-stimulated macrophages enter
848 HBV-replicating hepatocytes through CME (rapid mode) and macropinocytosis
849 (sustained mode). Endocytosed exosomes traffic to LEs/MVBs and fuse with LBPA-rich
850 ILVs. Trapped antiviral cargo in the ILVs are released to the cytosol via the back-fusion of
851 ILVs with the limiting membrane of LEs/MVBs (violet arrow). Alternatively, ILV-derived
852 exosomes release antiviral cargo via direct fusion with LEs/MVBs (blue arrow).

853

Figure 1

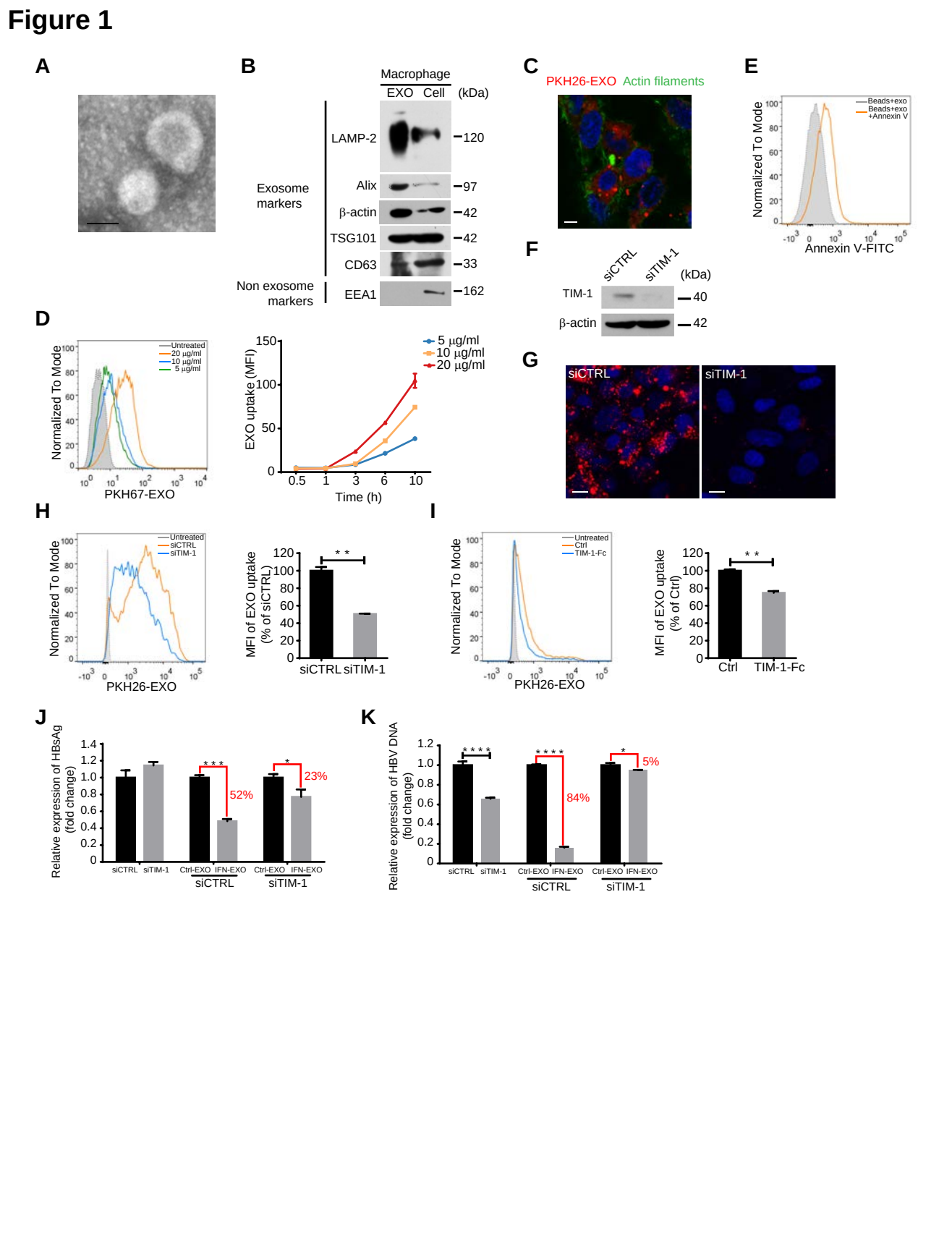
A
B
Macrophage
EXO Cell (kDa)
Exosome markers
LAMP-2 120
Alix 97
β-actin 42
TSG101 42
CD63 33
Non exosome markers
EEA1 162
C
PKH26-EXO Actin filaments
E
Normalized To Mode
Beads+exo
Beads+exo +Annexin V
Annexin V-FITC
D
Normalized To Mode
Untreated
20 μg/ml
10 μg/ml
5 μg/ml
PKH67-EXO
EXO uptake (MFI)
5 μg/ml
10 μg/ml
20 μg/ml
Time (h)
F
siCTRL siTIM-1 (kDa)
TIM-1 40
β-actin 42
G
siCTRL
siTIM-1
H
Normalized To Mode
Untreated
siCTRL
siTIM-1
PKH26-EXO
MFI of EXO uptake (% of siCTRL)
siCTRL siTIM-1
I
Normalized To Mode
Untreated
Ctrl
TIM-1-Fc
PKH26-EXO
MFI of EXO uptake (% of Ctrl)
Ctrl TIM-1-Fc
J
Relative expression of HBsAg (fold change)
52%
23%
siCTRL siTIM-1 Ctrl-EXO IFN-EXO Ctrl-EXO IFN-EXO
siCTRL siTIM-1
K
Relative expression of HBV DNA (fold change)
84%
5%
siCTRL siTIM-1 Ctrl-EXO IFN-EXO Ctrl-EXO IFN-EXO
siCTRL siTIM-1

Figure 2

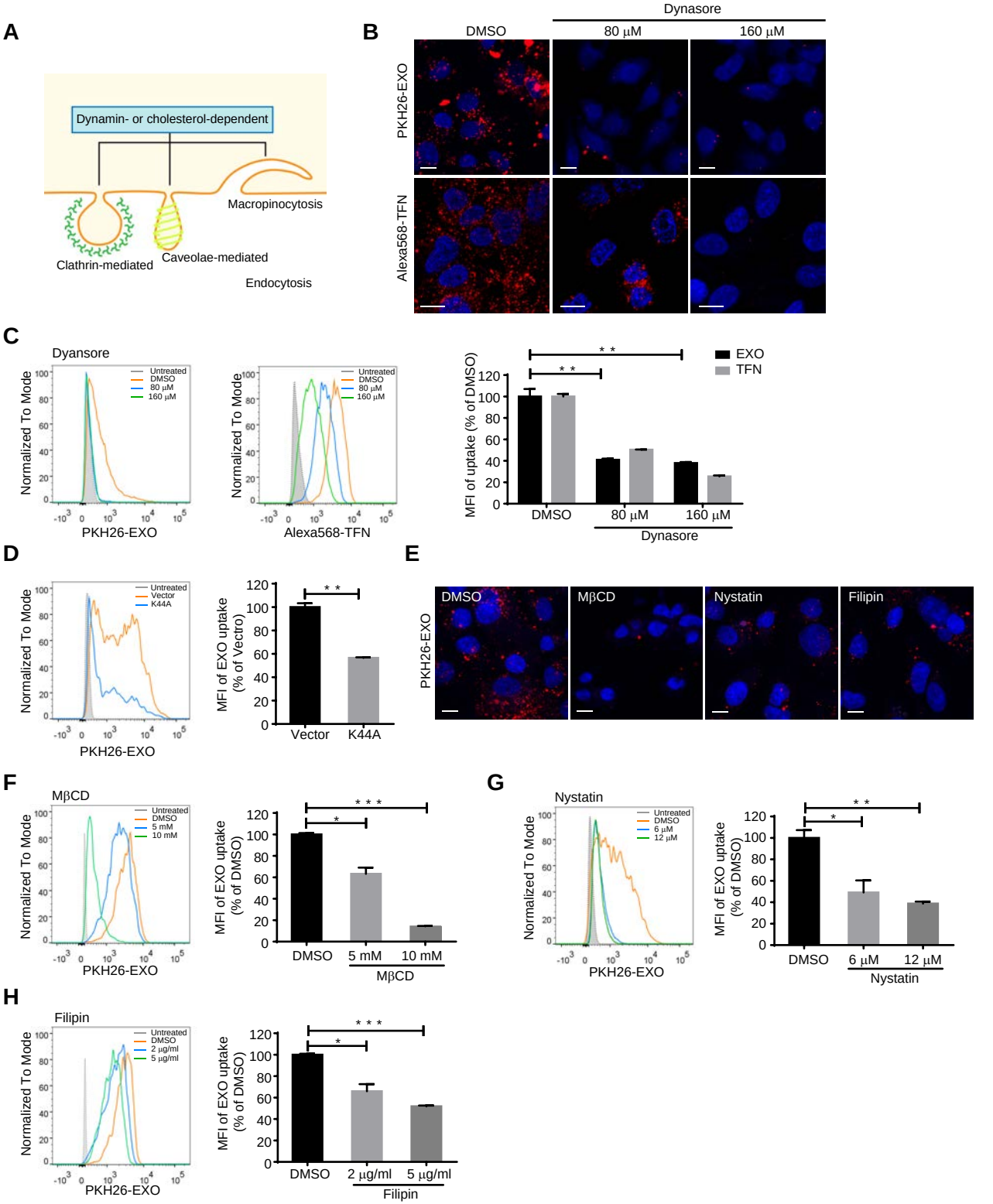
A
Dynamin- or cholesterol-dependent
Macropinocytosis
Clathrin-mediated
Caveolae-mediated
Endocytosis
B
Dynasore
DMSO
80 μM
160 μM
PKH26-EXO
Alexa568-TFN
C
Dyansore
Normalized To Mode
Untreated
DMSO
80 μM
160 μM
PKH26-EXO
Alexa568-TFN
MFI of uptake (% of DMSO)
EXO
TFN
D
Untreated
Vector
K44A
MFI of EXO uptake (% of Vectro)
E
DMSO
MβCD
Nystatin
Filipin
F
MβCD
5 mM
10 mM
MFI of EXO uptake (% of DMSO)
G
Nystatin
6 μM
12 μM
H
Filipin
2 μg/ml
5 μg/ml

Figure 3

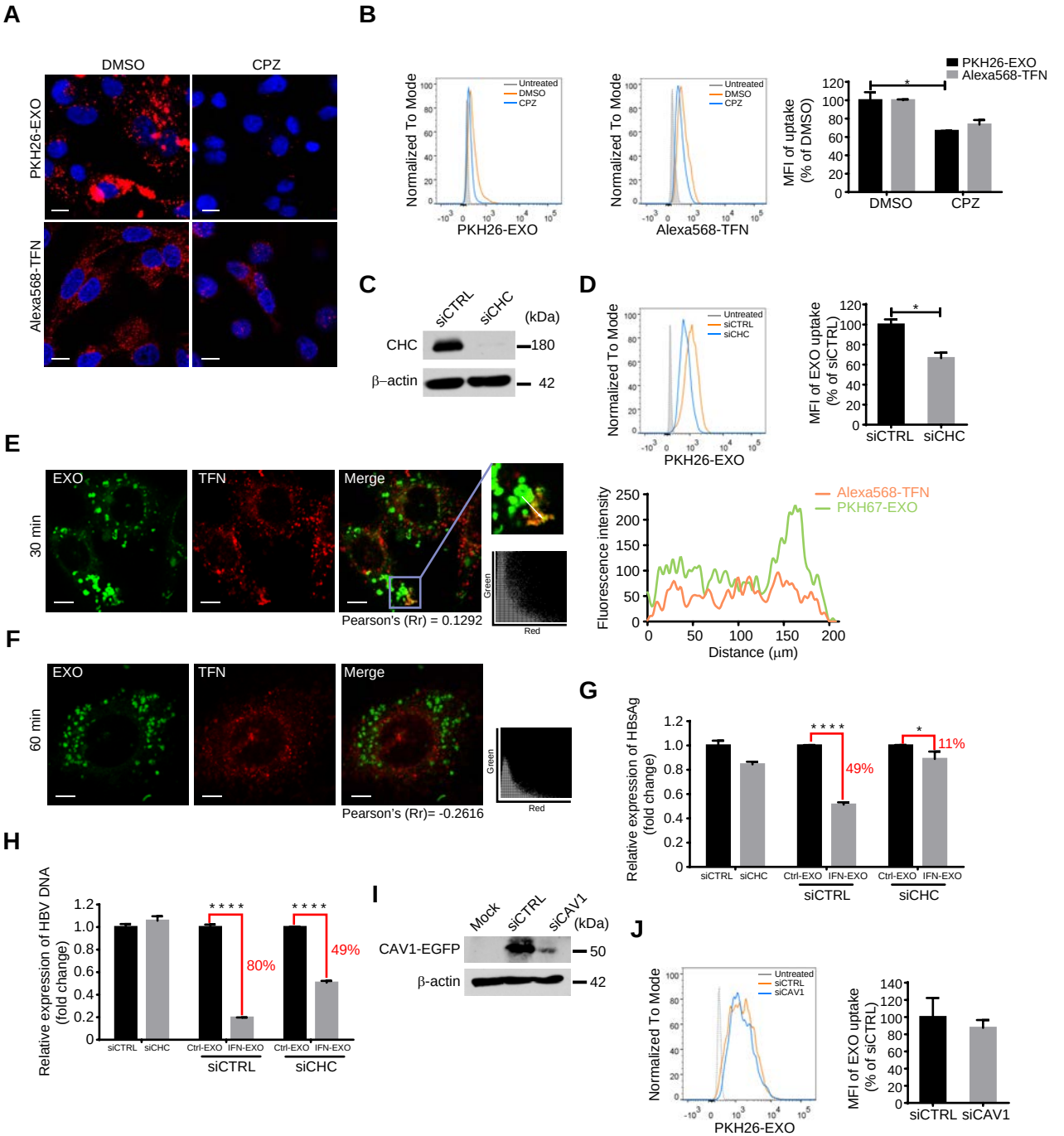
A
DMSO
CPZ
PKH26-EXO
Alexa568-TFN
B
Normalized To Mode
Untreated
DMSO
CPZ
PKH26-EXO
Alexa568-TFN
MFI of uptake (% of DMSO)
PKH26-EXO
Alexa568-TFN
DMSO
CPZ
C
siCTRL
siCHC
(kDa)
CHC
180
β–actin
42
D
Untreated
siCTRL
siCHC
PKH26-EXO
MFI of EXO uptake (% of siCTRL)
siCTRL
siCHC
E
30 min
EXO
TFN
Merge
Pearson's (Rr) = 0.1292
Green
Red
Alexa568-TFN
PKH67-EXO
Fluorescence intensity
Distance (μm)
F
60 min
EXO
TFN
Merge
Pearson's (Rr)= -0.2616
Green
Red
G
Relative expression of HBsAg (fold change)
49%
11%
siCTRL
siCHC
Ctrl-EXO
IFN-EXO
H
Relative expression of HBV DNA (fold change)
80%
49%
I
Mock
siCTRL
siCAV1
(kDa)
CAV1-EGFP
50
β-actin
42
J
Untreated
siCTRL
siCAV1
PKH26-EXO
MFI of EXO uptake (% of siCTRL)
siCTRL
siCAV1

Figure 4

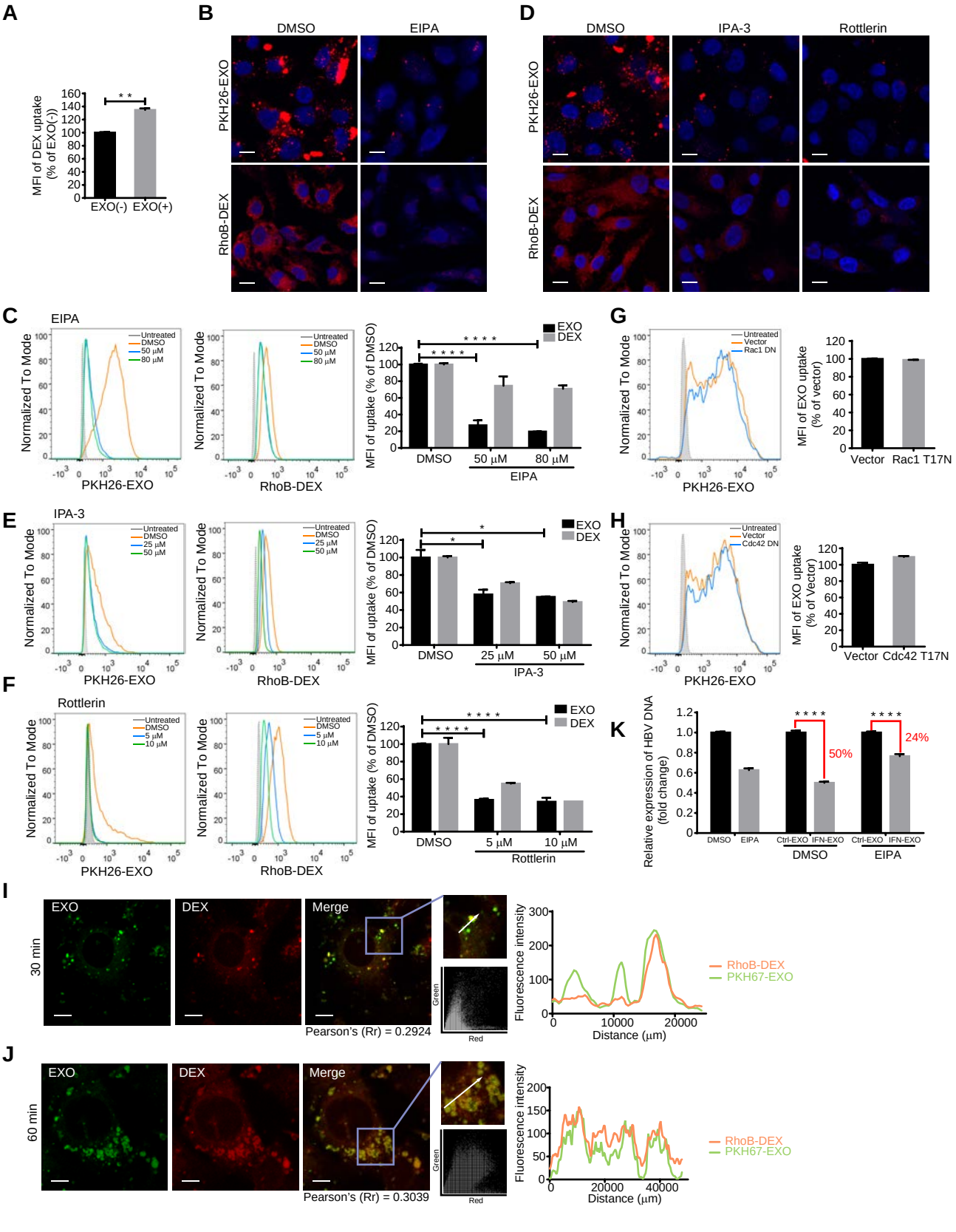
A
MFI of DEX uptake (% of EXO(-))
EXO(-) EXO(+)
B
DMSO
EIPA
PKH26-EXO
RhoB-DEX
D
DMSO
IPA-3
Rottlerin
C
EIPA
Normalized To Mode
Untreated
DMSO
50 μM
80 μM
PKH26-EXO
RhoB-DEX
MFI of uptake (% of DMSO)
EXO
DEX
DMSO
50 μM
80 μM
G
Rac1 DN
MFI of EXO uptake (% of vector)
Vector
Rac1 T17N
E
IPA-3
25 μM
50 μM
Cdc42 DN
Cdc42 T17N
F
Rottlerin
5 μM
10 μM
K
Relative expression of HBV DNA (fold change)
50%
24%
Ctrl-EXO
IFN-EXO
I
30 min
EXO
DEX
Merge
Pearson's (Rr) = 0.2924
Green
Red
Fluorescence intensity
Distance (μm)
RhoB-DEX
PKH67-EXO
J
60 min
Pearson's (Rr) = 0.3039

Figure 5

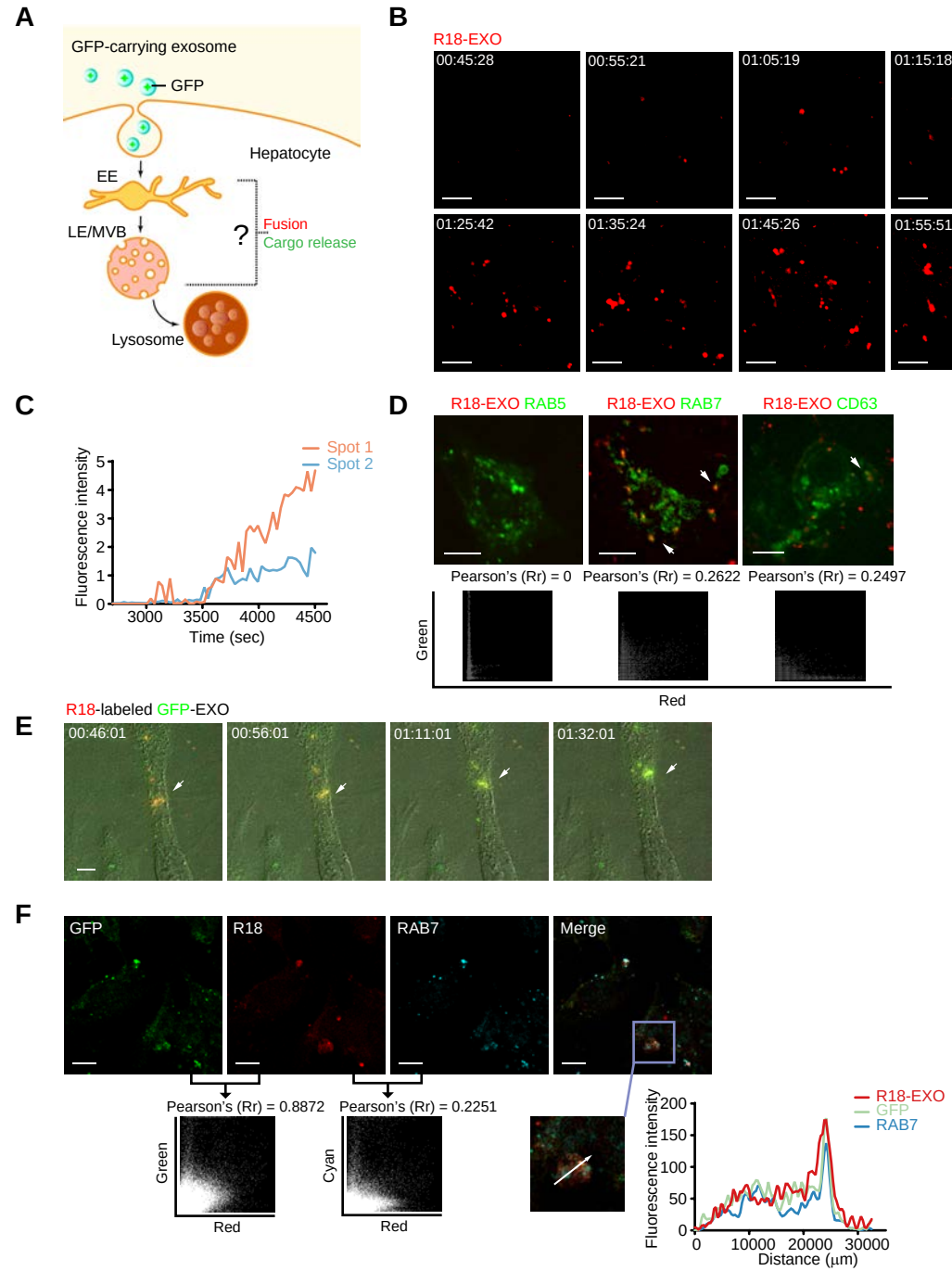
A
GFP-carrying exosome
GFP
Hepatocyte
EE
LE/MVB
?
Fusion
Cargo release
Lysosome
B
R18-EXO
00:45:28
00:55:21
01:05:19
01:15:18
01:25:42
01:35:24
01:45:26
01:55:51
C
Spot 1
Spot 2
Fluorescence intensity
Time (sec)
D
R18-EXO RAB5
R18-EXO RAB7
R18-EXO CD63
Pearson's (Rr) = 0
Pearson's (Rr) = 0.2622
Pearson's (Rr) = 0.2497
Green
Red
E
R18-labeled GFP-EXO
00:46:01
00:56:01
01:11:01
01:32:01
F
GFP
R18
RAB7
Merge
Pearson's (Rr) = 0.8872
Pearson's (Rr) = 0.2251
Green
Red
Cyan
Red
R18-EXO
GFP
RAB7
Fluorescence intensity
Distance (μm)

Figure 6

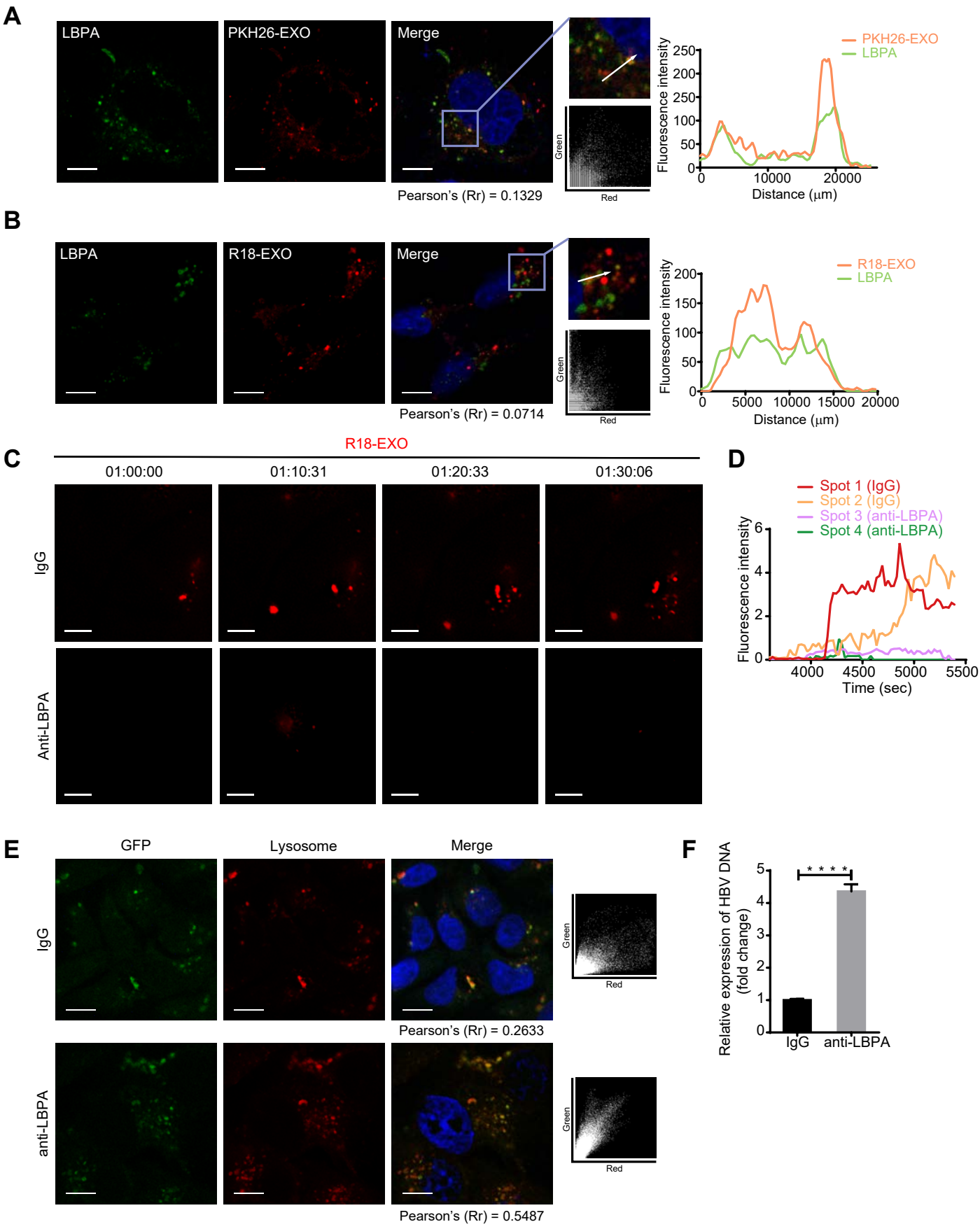
A
LBPA
PKH26-EXO
Merge
Pearson's (Rr) = 0.1329
Green
Red
Fluorescence intensity
Distance (μm)
PKH26-EXO
LBPA
B
LBPA
R18-EXO
Merge
Pearson's (Rr) = 0.0714
Green
Red
Fluorescence intensity
Distance (μm)
R18-EXO
LBPA
C
R18-EXO
01:00:00
01:10:31
01:20:33
01:30:06
IgG
Anti-LBPA
D
Spot 1 (IgG)
Spot 2 (IgG)
Spot 3 (anti-LBPA)
Spot 4 (anti-LBPA)
Fluorescence intensity
Time (sec)
E
GFP
Lysosome
Merge
IgG
Pearson's (Rr) = 0.2633
anti-LBPA
Pearson's (Rr) = 0.5487
Green
Red
F
Relative expression of HBV DNA (fold change)
IgG
anti-LBPA

Figure 7

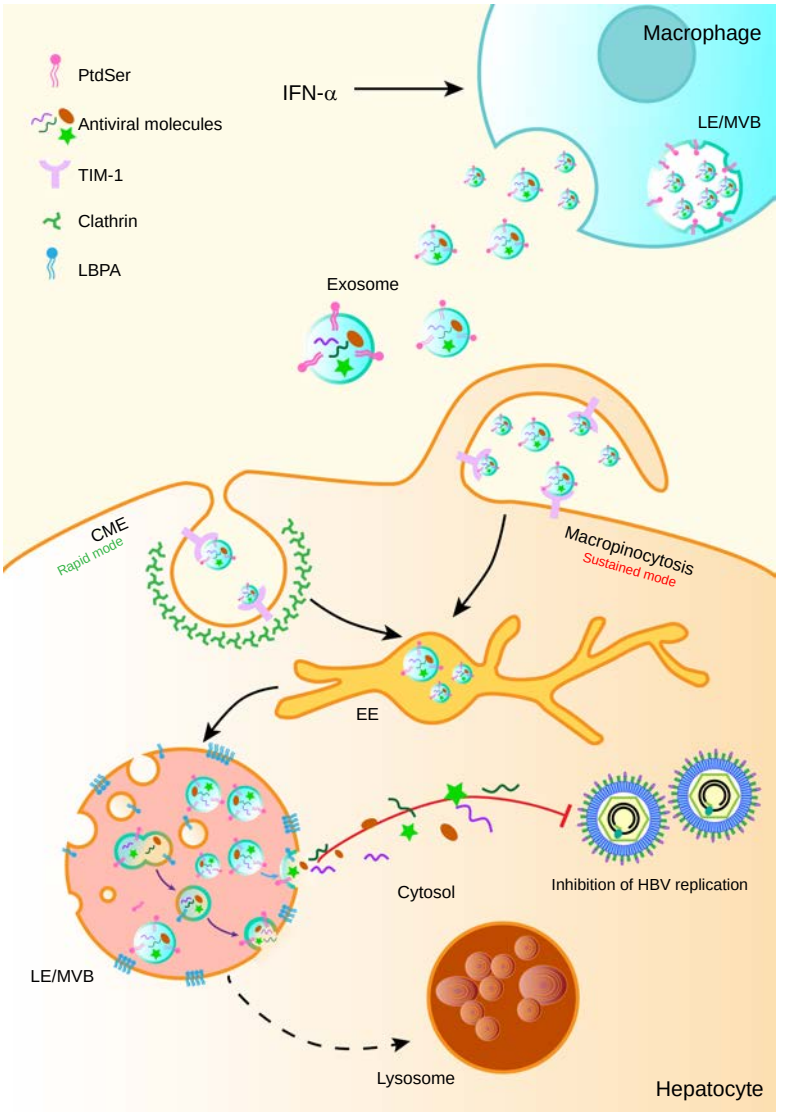
Macrophage
PtdSer
Antiviral molecules
TIM-1
Clathrin
LBPA
IFN-α
LE/MVB
Exosome
CME
Rapid mode
Macropinocytosis
Sustained mode
EE
Cytosol
Inhibition of HBV replication
LE/MVB
Lysosome
Hepatocyte